

# Evaluation of independent and cumulative fission product yields with gamma spectrometry

Kenneth Dayman<sup>1</sup> · Steven Biegalski<sup>1</sup> · Derek Haas<sup>2</sup> · Amanda Prinke<sup>2</sup> · Sean Stave<sup>2</sup>

Received: 15 June 2015 / Published online: 12 November 2015  
© Akadémiai Kiadó, Budapest, Hungary 2015

**Abstract** Fission product yields are critical data for a variety of nuclear science and engineering applications; however, independent yields have not been extensively measured to date. We have previously documented a methodology to measure the cumulative and independent fission product yields using gamma spectrometry and nuclide buildup and decay modeling, and numerical optimization. We have produced fission products by bombarding  $^{235}\text{U}$  with 14.1 MeV neutrons and made measurements of fission product yields. In this paper, we summarize our approach, describe initial experiments, and present preliminary results where we have determined nine fission product yields for long-lived nuclides.

**Keywords** Fission product yields · Optimization · Gamma spectrometry

## Introduction

Accurate modeling of the buildup and decay of fission products (FP) during and after fission is a fundamental part of many nuclear engineering applications. Accordingly, fission product yields (FPY), which describe the likelihood of any particular fission product being produced by the fission of a particular fissionable nuclide, e.g.,  $^{235}\text{U}$  or  $^{238}\text{U}$ ,

by an incident particle of some energy, e.g., a thermal neutron, are critical fundamental data for nuclear science.

Despite their importance, there is a lack of direct measurements of FPY, and existing datasets such as ENDF and JEFF have shortcomings [1, 2]. Many values do not agree between datasets and the reported uncertainties fail to capture the true uncertainty in the reported values, i.e., the confidence intervals reported in different datasets do not overlap even when large coverage factors are used [3].

For these reasons, we have pursued new measurements of FPY, with focus placed on the measurement of *independent* fission product yields that have been determined with semi-empirical models to data [4–6]. In this paper, we summarize an analysis method based on Bayesian inference capable of determining independent and cumulative FPY from series of gamma-ray spectra collected of irradiated fissionable material, as well as the initial results of measurements made of highly-enriched  $^{235}\text{U}$  with 14 MeV neutrons.

## Background

To date, the majority of FPY measured have focused on thermal or fission-spectrum neutron-induced fission; however, there have been some measurements of FPY from fission initiated by 14 MeV neutrons [7, 8]. Like previous work measuring FPY, these authors determine cumulative/chain yields as opposed to independent/direct yields, i.e., the likelihood of a FP arising directly from fission without the contribution of decaying parent nuclide(s).

There are several difficulties in attempting to measure independent FPY. First, it is difficult to differentiate between the contribution made from fission and contributions from the decay of parent nuclides. This problem is

---

✉ Kenneth Dayman  
kenneth.dayman@gmail.com

<sup>1</sup> University of Texas at Austin, 10100 Burnet Rd., Bldg. 159, Austin, TX 78758, USA

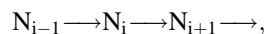
<sup>2</sup> Pacific Northwest National Laboratory, 902 Battelle Boulevard, Richland, WA 99352, USA

coupled with the constant changes undergone by the FP inventory in a sample during and following irradiation. Determining the FP composition in an irradiated material is complicated by the large number of FP in a sample. Waiting for the sample to decay reduces this complexity by virtue of reducing the number of nuclides in the total inventory; however, this reduction makes analysis of many short- and medium-lived FP impossible. Therefore, the analyst must determine values only for long-lived nuclides at the end of FP decay chains.

## Theory

We have developed a method to measure independent and cumulative FPY of FP decay chains, which we have previously documented [3]. This section provides a summary of the method used to determine FPY; however, we refer the reader to [3] for a more complete treatment.

First, FP in the sample after irradiation are identified using the usual methods of gamma spectroscopy [9]. For each radionuclide identified, the activity at the beginning of counting for every member of the decay chain is calculated simultaneously as a system. For a three-nuclide system,



the buildup and decay of nuclides  $N_{i-1}$ ,  $N_i$ , and  $N_{i+1}$  is described by the system of equations shown below.

$$\frac{d}{dt}(N_i) = \lambda_{i-1}N_{i-1} - \lambda_i N_i \quad i = 1, 2, \dots \quad (1)$$

These equations are solved, multiplied by  $\lambda_i$  to get activity as a function of time, integrated to get the number of counts, and then rearranged to give an expression for the activity at the beginning of counting.

The same chain of FP may be modeling during and after irradiation. This model (see Eq. (2)) depends on the neutron flux, fission cross section, decay constants for all nuclides in the model, cross sections for all reactions, and fission product yields. The cumulative FPY is used to model the buildup of the first nuclide in the decay chain, and the independent FPY are used for all subsequent nuclides in the chain. Solving this system leads to a predicted activity over time of each nuclide in the chain.

$$\frac{d}{dt}(N_i) = \phi \sum_f \chi_i + \lambda_{i+1}N_{i+1} - \lambda_i N_i - \phi \left( \sum_j N_j \sigma_j \right) \quad i = 1, 2, \dots \quad (2)$$

The predicted activities of each nuclide,  $R_\theta(t)$ , given assumed values of the input parameters,  $\theta$ , are compared to the measured values,  $A(t)$ , and the values  $\theta$  are altered to estimate the best-fit values. These best-fit values are

defined in the Bayesian sense, which incorporates the prior distribution values and uncertainty,  $\bar{\theta}$  and  $u(\theta)$ , shown in Eq. (3) for  $N$  quantities to be estimated. The matrix  $W$  is a diagonal matrix of weighting terms for each comparison,  $W_{ii} = (u(R_\theta(t))^2 + u(A(t))^2)^{-1}$ . Equation (3) is solved using a numerical optimization algorithm.

$$\hat{\theta} = \underset{\theta \in \mathbb{R}_+^N}{\operatorname{argmin}} \left\{ \|W(R_\theta(t) - A(t))\|_2^2 + \sum_{j=1}^N \left( \frac{(\theta_j - \bar{\theta}_j)^2}{2u(\theta_j)^2} \right) \right\} \quad (3)$$

In The problem shown in Eq. (3) presents two primary difficulties: (1) the objective function does not vary smoothly with the measured activities,  $A(t)$ , and parameters used to compute the predicted FP activities,  $R_\theta(t)$  due to the noise in the measured activities; and (2) the derivatives of the objective are not available analytically. All derivatives are estimated using central differencing; however, these local estimates may be skewed by the noise and discontinuities in the function and may not adequately represent the function's global behavior.

In this work we have primarily solved Eq. (3) using the Levenberg-Marquardt (LM) method, which is a variation of Newton's method [10]. Due to the difficulties in solving Eq. (3), we employed two alternative solution algorithms to assess their ability to find the global minimum of Eq. (3)<sup>1</sup>. In addition to the LM method, Newton's method (NM) and the Nelder-Mead simplex direct search were used. Newton's method is a standard root-finding method used for optimization, and it gives excellent local convergence properties. The Nelder-Mead algorithm is a gradient-free method that avoids the need to estimate derivatives numerically, but it does not give guarantees of convergence in most instances [11, 12].

The parameters shown in Eqs. (1) and (2) carry uncertainty that must be propagated through Eq. (3) to obtain the uncertainty on the estimate of  $\hat{\theta}$ . This is done by describing each of the parameters with a probability distribution, combining these distributions into a single, multivariate distribution that incorporates correlations between the parameters, and using this distribution as an input for a Monte Carlo algorithm. The multivariate distribution is sampled, Eq. (3) is solved using these values, and the process is repeated. The collection of estimates for  $\hat{\theta}$  gives an approximation for the distribution of  $\hat{\theta}$  (the posterior distribution in Bayesian parlance). From these distributions, summary statistics, e.g., mean and standard deviation, are computed.

<sup>1</sup> The optimization problem shown in Equation (3) is convex and thus has a global minimum. Convexity follows from the non-negative sum of two convex functions (a norm and a parabola) defined on a convex domain,  $\mathbb{R}_+^N$ . See [10] for a complete discussion.

## Experiment

This section summarizes the experiment conducted to produce FP from  $^{235}\text{U}$  with 14 MeV neutrons, collection of gamma spectra, and the analysis of these spectra to obtain approximate posterior distributions for fission product yields.

### Data Collection

A thin foil target was cut from highly-enriched metallic  $^{235}\text{U}$ . The mass was determined to be  $220 \pm 1$  mg, and the material was confirmed to be more than 99 % isotopically pure. This target was bombarded with 14.1 MeV neutrons obtained from a commercially available neutron generator with a measured maximum neutron flux of approximately  $1 \times 10^9 \text{ cm}^{-2}\text{s}^{-1}$  for approximately 333 s. A pneumatic rabbit system was used to transport the irradiated material to an isolated location for gamma counting. A radiation protection survey was required prior to transport, and this survey increased the minimum possible time between end-of-irradiation and the beginning of counting to approximately 5 min.

Following a decay time of 297 s, gamma-rays were measured using a Canberra BE6530 broad energy high-purity germanium detector with composite a carbon window attached to a Canberra 2002 CSI pre-amplifier and Lynx multichannel analyzers to collect list-mode data. Data was collected for approximately 166 h. The list-mode data was parsed offline to create 12, 3, 1-h, and 20-min time cuts.

### Data analysis

The peak detector efficiency was calculated in the usual way using a multi-gamma standard containing  $^{210}\text{Pb}$  (46.5 keV),  $^{241}\text{Am}$  (59.5 keV),  $^{109}\text{Cd}$  (88.0 keV),  $^{57}\text{Co}$  (122.1, 136.5 keV),  $^{139}\text{Ce}$  (165.9 keV),  $^{203}\text{Hg}$  (279.2 keV),  $^{113}\text{Sn}$  (391.7 keV),  $^{85}\text{Sr}$  (514.0 keV),  $^{137}\text{Cs}$  (661.7 keV),  $^{88}\text{Y}$  (898, 1836.1 keV), and  $^{60}\text{Co}$  (1173.2, 1332.5 keV), which was counted for 1300 s. This gives the curve  $\epsilon(E)$ .

The target’s high density (approximately 19 g/cc) gives large attenuation coefficients (approximately  $37 \text{ cm}^{-1}$  at 100 keV), and self-attenuation must be corrected. The expected attenuation factor is easily calculated as

$$\text{Attn}(E) = \frac{\int_0^x e^{-\mu(E)s} ds}{\int_0^x ds} = \frac{1 - e^{-\mu(E)x_{\text{eff}}}}{\mu(E)x_{\text{eff}}}, \quad (4)$$

where  $x_{\text{eff}}$  is the effective averaged distance a photon incident on the detector will travel through the foil.

A 12-h cut of the list mode data was taken from the end of data collection. The expected number of counts were

predicted for the 143, 163, 186, and 205 keV peaks of  $^{235}\text{U}$ . The ratio of the actual to predicted number of counts gives the attenuation factor at each of the four energies. Using each value, the effective foil thickness was calculated, and the four results averaged to obtain a mean value. Using this estimate, the full attenuation curve was extrapolated using NIST mass attenuation coefficients [13]. The product of the peak efficiency and attenuation curves gives the effective efficiency curve,  $\epsilon_{\text{eff}}(E) = \text{Attn}(E)\epsilon(E)$ . Figure 1 shows the peak detector efficiency in blue, self-attenuation function in red, and the effective efficiency in green.

The effective efficiency was used to calculate the activity at beginning of counting for each identified FP. When chains of FP were identified, the activities of all nuclides in the chain were found simultaneously as a system in order to account for nuclide transmutation [see Eq. (1)].

The neutron flux and FPY are not independent in the system of Eq. (2). Thus, the time-averaged neutron flux was found using  $^{99}\text{Mo}$  as a standard, treating the cumulative yield as an uncertain input. This result was then used in all subsequent calculations where FPY were determined.

## Results and discussion

In this section, we discuss the time-averaged neutron flux calculated using the LM, NM, and Nelder-Mead algorithms. We then present the fission product yield estimates made to date.

### Flux Estimation

Using the parameters shown in Table 1, the time-averaged neutron flux was determined using the LM, NM, and Nelder-Mead algorithms. Production of  $^{99}\text{Mo}$  was modest, leading to a maximum activity of 10.56 Bq and poor counting statistics. The relative uncertainty in the eleven measurements ranged between 6.2 and 52.6 %. The 14.1 MeV  $^{235}\text{U}$  fission cross section was interpolated from ENDF/B-VII data [1].

The neutron flux estimates made with the three solvers are given in Table 2. Flux estimates made using Newton’s method ranged from approximately  $2.0 \times 10^8$  to  $1.5 \times 10^{15} \text{ cm}^{-2}\text{s}^{-1}$ . We attribute this large range to instability in the method induced by poor conditioning of the Hessian matrix used for Newton updating [10]. The NM flux estimates fell into two intervals:  $[2.05 \times 10^8, 2.75 \times 10^8]$  and  $[3.81 \times 10^{13}, 1.54 \times 10^{15}]$ . The second interval, attributed to samples that gave rise to poorly-conditioned Hessian matrices, were considered outliers and excluded from the computation of the summary statistics reported in Table 2. After

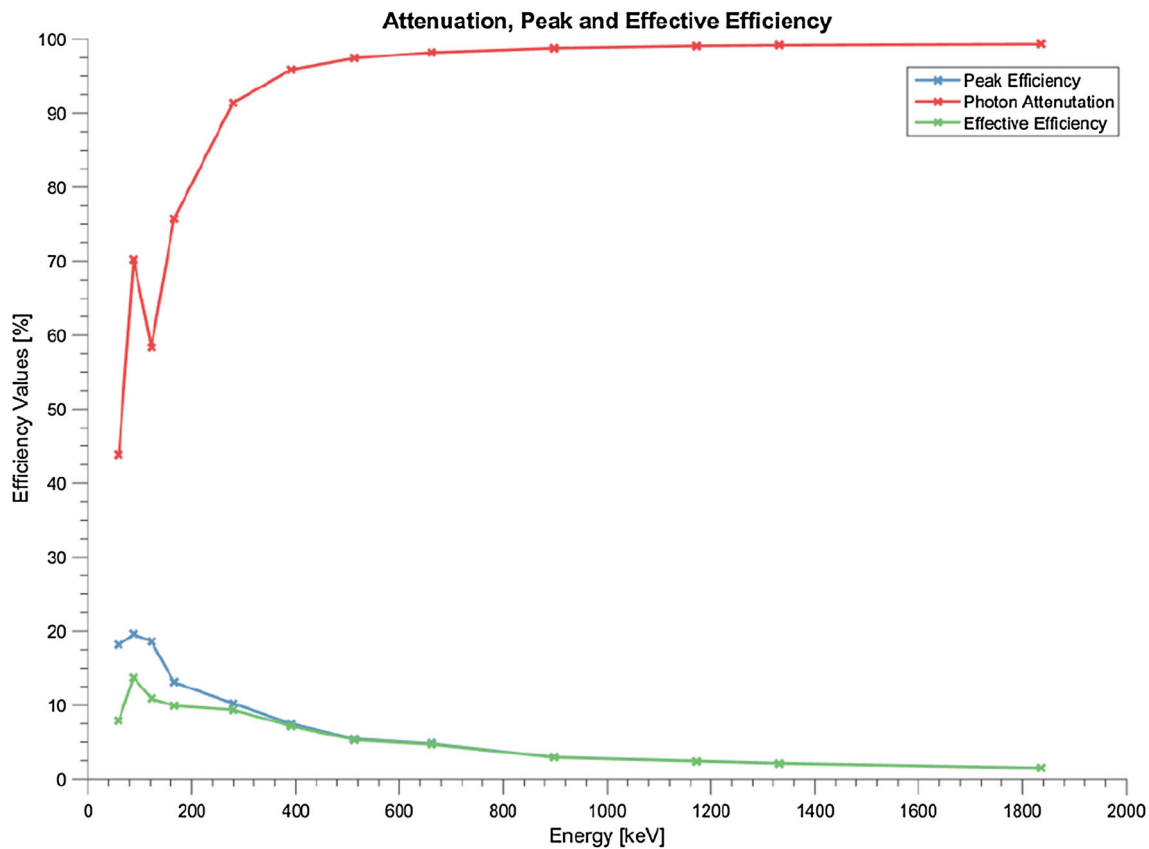


**Fig. 1** Peak detector efficiency curve (blue), extrapolated attenuation factors calculated using the estimated effective thickness,  $x_{\text{eff}}$ , and NIST attenuation coefficients (red), and effective efficiency curve

(green). The large dip in the red and green curves at 115 keV is due to the K-absorption shell of  $^{235}\text{U}$ . (colour figure online)

**Table 1** Parameters and associated uncertainty used to calculate the time-averaged neutron flux during sample irradiation. For brevity, the eleven measurements of  $^{99}\text{Mo}$  derived from eleven 12-h spectra parsed from the dataset collected following irradiation (see Section 4) are averaged together. Relative uncertainties in activity were especially large near the end of collection due to low count rate (less than 2 net counts in the 739.5 keV peak).

Parameter	Value	Relative Uncertainty (%)
Measured activities	6.2 Bq	17.0
Irradiation time	333.0	0.3
Decay constant	$2.9 \times 10^{-6} \text{ s}^{-1}$	<0.1
Cumulative fission yield	5.2 %	2.9
$^{235}\text{U}$ cross section	2.1	2.0
$^{235}\text{U}$ mass	220 mg	0.1
$^{235}\text{U}$ density	$19.0 \text{ g cm}^{-3}$	1.6

removing these outliers, results from the three solvers agreed exceptionally well, which indicates the results are based on reality and are not based on numerical/solution artifacts. The mean relative uncertainty in the flux estimate

**Table 2** Time-averaged neutron flux estimations made using 5000 Monte Carlo samples of 17-dimensional input space. Normal distributions were fit to sampled posterior distributions using the sample mean and variance. The mean value and standard uncertainty are reported.

Solver	Estimated flux $\text{cm}^{-2}\text{s}^{-1}$
LM	$(2.3565 \pm 0.1113) \times 10^8$
Nelder-Mead	$(2.3538 \pm 0.1109) \times 10^8$
NM†	$(2.3606 \pm 0.1101) \times 10^8$

† Results using Newton's method only include 435 samples as others went to extreme values ( $> 5 \times 10^{13}$ ) due to instability of the method, attributed to large condition numbers.

is 4.70 %. The uncertainty in output is much less than the uncertainty in inputs. We attribute this reduction to using eleven activity measurements, which effectively “averages out” measurement bias through the optimization formulation. The contribution of each source of uncertainty may be quantified by computing the uncertainty budget—our method and the results of the calculation are presented in a previous publication [3].

As shown in Table 2, the values are consistent between the three solvers, and the LM value,  $(2.3565 \pm 0.1113) \times 10^8 \text{ cm}^{-2}\text{s}^{-1}$ , are consistent with the maximum specified flux value for the generator (see Section 4).

### Estimation of fission product yields

Following an initial analysis of the 12-h cuts of the dataset collected following irradiation (see Section 4), gamma-ray signatures of the following radionuclides were identified:  $^{95}\text{Zr}/^{95}\text{Nb}$ ,  $^{99}\text{Mo}$ ,  $^{127}\text{Sb}$ ,  $^{131}\text{I}$ ,  $^{140}\text{Ba}/^{140}\text{La}$ , and  $^{147}\text{Nd}$ <sup>2</sup>. Counting statistics were poor: the majority of the observed photopeaks only contained several hundred counts or less, corresponding to net count rates less than 0.1 counts per second. Calculation of nuclide activity at the beginning of counting using different characteristic photons gives inconsistent results, therefore the results obtained using multiple photons were aggregated using a multi-dimensional generalization of the bootstrap median algorithm, which is based on an idea proposed by Helene and Vanin [14]. The following nuclides were identified using 20-min cuts of the dataset:  $^{89}\text{Kr}/^{89}\text{Rb}$ ,  $^{94}\text{Y}$ ,  $^{104}\text{Tc}$ ,  $^{130}\text{Sb}$ ,  $^{134}\text{Te}/^{134}\text{I}$ ,  $^{138}\text{Xe}/^{138}\text{Cs}$ ,  $^{146}\text{Ce}/^{146}\text{Pr}$ .

First, a multivariate normal distribution,  $\mathcal{N}(x|\mu, \Sigma)$ , is attributed to each calculated activity, using the determined value of each nuclide in the chain for  $\mu$ , the square of the standard uncertainty as the diagonal of  $\Sigma$ , and the off-diagonal terms are given by  $\frac{\partial y}{\partial x} u(x)^2$ , where  $y$  and  $x$  are activities of different nuclides in the chain and  $u(x)$  is the standard uncertainty in the activity  $x$ . Many samples are drawn from these distributions and collected. Subsets of these datapoints are randomly drawn (bootstrapping) and the median is calculated for each. Finally, a normal distribution is fit to the collection of median values, and the parameters of this fit is the reported value. As discussed by Helene and Vanin, the median is robust to outliers, and using the bootstrapping procedure allows the uncertainty of each measurement to be explicitly considered.

The fission product yields for each decay chain were estimated using ten-thousand Monte Carlo samples. When multiple nuclides in the chain were observed, e.g.,  $^{140}\text{Ba}/^{140}\text{La}$ , the cumulative yield was determined for the parent and the independent yield(s) were determined for all subsequent daughter product(s). The results are summarized in Table 3. As shown in the last column, results obtained for FP in decay chains are strongly correlated. Reporting the correlation reduces the total range of likely values that the FPY can take.

The measured yields of  $^{89}\text{Kr}$  and  $^{89}\text{Rb}$  were within 3.9 and 46.7 % of the literature values, respectively. Good counting statistics were obtained due to the high specific activity of the nuclides, and there is considerable uncertainty in the true FPY of  $^{89}\text{Rb}$ —the literature-derived uncertainty is 50.6 %. This results suggests that further measurements of FPY for  $^{89}\text{Kr}$  and  $^{89}\text{Rb}$  and possibly updating the nuclear data is warranted.

The measured value for the FPY of  $^{94}\text{Y}$  is approximately 24 % smaller than the literature value. No significant source of bias is evident, and counting statistics were within 5 %. Due to the short half-life, it is unlikely that the existing literature values are based on measurements, which have been performed with radiochemical separations and destructive analysis, but rather are likely based on nuclear models evaluating using historical data. As the nuclear data, e.g., branching ratios, have been updated, the existing FPY values may no longer be valid.

The values obtained for  $^{95}\text{Zr}$  and  $^{95}\text{Nb}$  differ significantly from existing values (the value for Nb is approximately 3900 % greater than the value used in the prior distribution). We attribute the errant result to an overestimation of activity stemming from an unresolved spectral interference. In addition, the expected value for the FPY of Nb is very small: the number of Nb nuclei produced directly from fission (captured by the independent yield) is much smaller than the nuclei produced from the decay of the parent nuclei (captured by the cumulative yield of Zr), and this additional Nb activity is easily lost in the noise of the activity measurements.

The values obtained for  $^{104}\text{Tc}$ ,  $^{127}\text{Sb}$ , and  $^{130}\text{Sb}$  are fairly commensurate with existing values. In addition, the result for  $^{131}\text{I}$  somewhat agrees with the existing value, and there may be an unresolved spectral interference and associated activity overestimation.

The short half-lives and large specific activities of  $^{134}\text{Te}$  and  $^{134}\text{I}$  led to an average precision in the measured activities of the two-nuclide chain less than 1 %. The determined values are commensurate with the value obtained from the literature, differing by 0.01 and 1.06 percentage points, respectively.

The cumulative yield of  $^{138}\text{Xe}$  was underestimated relative to existing values and the independent yield of  $^{138}\text{Cs}$  was overestimated relative to the literature. The overestimation of the daughter independent yield is attributed to the underestimation of the cumulative yield of the parent nuclide (attributed to uncertainty in the measured activities), which is balanced by an overestimation of the independent yield of the daughter. Similar behavior is observed in the results obtained for the  $^{140}\text{Ba}/^{140}\text{La}$  decay chain.

The measured values for  $^{146}\text{Ce}$  and  $^{146}\text{Pr}$  are commensurate with prior values, differing by 0.36 and 0.17 percentage points, respectively. As in previous cases, an

<sup>2</sup> Parent/daughter chains are written with a slash.



**Table 3** Results of fission product yields of 14.1 MeV-neutron-induced fission of  $^{235}\text{U}$ . The values used in the prior distribution (mean and standard deviation), assembled from three major data sources, are also reported for reference.

Nuclide	Ind./cum. yield	Prior statistics (%)	Calculated value (%)	Correlation $r_{jk}$
$^{89}\text{Kr}$ (3.2 m)	C	$3.32 \pm 0.39$	$3.19 \pm 0.15$	+0.93
$^{89}\text{Rb}$ (15.2 m)	I	$0.75 \pm 1.14$	$1.10 \pm 0.05$	+0.93
$^{94}\text{Y}$ (18.7 m)	C	$5.05 \pm 2.81$	$3.82 \pm 0.17$	–
$^{95}\text{Zr}$ (64.0 d)	C	$5.14 \pm 0.56$	$11.98 \pm 0.51$	–0.94
$^{95}\text{Nb}$ (35.0 d)	I	$0.001 \pm 0.002$	$0.04 \pm 0.001$	–0.94
$^{104}\text{Tc}$ (18.3 m)	C	$2.47 \pm 1.71$	$1.87 \pm 0.08$	–
$^{127}\text{Sb}$ (3.9 d)	C	$2.08 \pm 0.95$	$1.57 \pm 0.07$	–
$^{130}\text{Sb}$ (39.5 m)	C	$1.45 \pm 3.14$	$0.84 \pm 0.04$	–
$^{131}\text{I}$ (8.0 d)	C	$4.11 \pm 0.49$	$6.00 \pm 0.27$	–
$^{134}\text{Te}$ (41.8 m)	C	$2.37 \pm 1.66$	$2.38 \pm 0.10$	+0.99
$^{134}\text{I}$ (52.5 m)	I	$1.06 \pm 1.05$	$2.12 \pm 0.09$	+0.99
$^{138}\text{Xe}$ (14.1 m)	C	$3.40 \pm 2.87$	$2.83 \pm 0.12$	+0.95
$^{138}\text{Cs}$ (33.4 m)	I	$0.47 \pm 1.28$	$1.83 \pm 0.08$	+0.95
$^{140}\text{Ba}$ (12.8 d)	C	$4.49 \pm 0.38$	$4.18 \pm 0.74$	–0.78
$^{140}\text{La}$ (1.7 d)	I	$0.03 \pm 0.06$	$0.46 \pm 0.46$	–0.78
$^{146}\text{Ce}$ (13.5 m)	C	$2.17 \pm 2.03$	$1.81 \pm 0.08$	+0.52
$^{146}\text{Pr}$ (24.2 m)	I	$0.07 \pm 0.16$	$0.24 \pm 0.02$	+0.52
$^{147}\text{Nd}$ (11.0 d)	C	$1.64 \pm 0.14$	$9.41 \pm 0.11$	–

underestimation in the FPY of the parent nuclide coincides with an overestimation in the FPY of the daughter nuclide. It should be noted that this correlation is not necessarily causation. A separate factor, such as spectral interference, could drive an overestimation of a poorly measured and/or poorly understood daughter nuclide and the FPY of the parent is adjusted during the simultaneous solution.

Finally, the result for  $^{147}\text{Nd}$  is very different than existing values found in the literature, which we attribute to poor counting statistics, whose relative uncertainty ranged from approximately 2 to 91 %.

In summary, while measured values differed (sometimes greatly) from existing values, the distribution of over- and under-estimations suggest that no system biases are present in the analysis, and the developed methodology is a valid approach for the determination of independent and cumulative FPY using gamma-ray spectrometry. Further validation of the methodology and additional measurements should be pursued in order to obtain results suitable for updating nuclear datasets.

## Conclusion

We have developed a method appropriate for measuring the activity of FP (especially short-lived nuclides) following irradiation and the estimation of cumulative and independent fission product yields. Our method relies on flexible modeling of FP during and after irradiation and comparing these predicted results to measured results. This comparison is combined with prior information taken from

the existing literature to form the objective of a convex optimization problem.

With attention to flexibility and future work, we have developed multiple solution algorithms for the problem described in Eqs. (2) and (3). Our implementation allows the user to fully specify time-varying neutron flux, e.g., pulses or cyclic irradiation as used by in cyclic neutron activation analysis or commercial reactor operations. In addition, the neutron spectrum may be implicitly specified by the user through the definition of the nuclear data values appearing in Eq. (2). Finally, our method allows the user to solve for any quantity in Equation (2), such as neutron flux, cross sections, branching ratios, decay constants, or nuclide concentrations.

We have produced FP by bombarding a  $^{235}\text{U}$  metal foil with 14.1 MeV neutrons obtained from a neutron generator and measuring the activities of several long-lived FP using list-mode spectral data collected using a high-purity germanium detector.

**Acknowledgments** This material is based upon work supported by the U.S. Department of Homeland Security under Grant Award Number, 2012-DN-130-NF0001-02. The views and conclusions contained in this document are those of the authors and should not be interpreted as representing the official policies, either expressed or implied, of the U.S. Department of Homeland Security.

## References

1. Chadwick MB, Herman M et al (2011) Nucl Data Sheets 112:28872996

2. Koning A, Dean C, Fischer U et al (2013) Validation of the JEFF 3.1 nuclear data library: JEFF report 23. Nuclear energy agency, Paris
3. Dayman K, Biegalski S, Haas D (2015) Determination of short-lived fission products yields with gamma spectrometry. *J Radioanal Nucl Chem*. DOI. doi:[10.1007/s10967-015-3993-9](https://doi.org/10.1007/s10967-015-3993-9)
4. Wahl AC (1962) *Phys Rev* 126:1112
5. Wahl AC (1980) *J Radioanal Nucl Chem* 55:111
6. Wahl AC (1988) *At Nucl Data Tables* 39:1
7. MacInnes M, Chadwick MB, Kawano T (2011) *Nucl Data Sheets* 112:3135
8. Laurec J, Adam A, Bruyne T et al (2010) *Nucl Data Sheets* 112:3135
9. Gilmore G (2008) *Practical gamma ray spectrometry*. Wiley, West Sussex
10. Boyd S, Vandenberghe L (2004) *Convex optimization*. Cambridge University Press, Cambridge
11. Nelder JA, Mead R (1965) *Comput J* 7:308
12. Lagarias JC, Reeds JA, Wright MH, Wright PE (1998) *SIAM J Optim* 9:112
13. Hubbell JH, Seltzer SM (2004) Tables of X-ray mass attenuation coefficients and mass energy-absorption coefficients from 1 keV to 20 MeV for elements Z = 1 to 92 and 48 additional substances of dosimetric interest, NISTIR 5632
14. Helene O, Vanin VR (2002) *Nucl Instrum Methods A* 481:626–631